Influence of Service-Induced Microstructural Changes on the Aging Kinetics of Rejuvenated Ni-Based Superalloy Gas Turbine Blades

E. Lvova and D. Norsworthy

(Submitted 17 January 2000)

Rejuvenation of Ni-based superalloy gas turbine blades is widely and successfully employed in order to restore the material microstructure and properties after service at high temperature and stresses. Application of hot isostatic pressing (HIP) and re-heat treatment can restore even a severely overaged blade microstructure to practically "as-new" condition. However, certain service-induced microstructural changes might affect an alloy's behavior after the rejuvenated blades are returned to service. It was found that advanced service-induced decomposition of primary MC carbides, and the consequent changes of the γ-matrix chemical composition during the rejuvenation, can cause a considerable acceleration of the aging process in the next service cycle. The paper will discuss the influence of the previous microstructural deterioration on the aging kinetics of rejuvenated gas turbine blades made from IN-738 and conventionally cast GTD-111 alloys.

Keywords gas turbine blades, HIP, IN738 alloy, nickel-based superalloys

1. Introduction

Gas turbine blades made from Ni-based superalloys experience the effect of high temperatures and stresses during service, which inevitably causes various microstructural changes. The microstructure deterioration can lead to a degradation of mechanical properties, such as tensile strength and creep resistance. Extensive studies have shown that prolonged thermal and stress exposure causes overaging of the alloy microstructure, that is, γ'-phase coarsening and coalescence, formation of continuous secondary $M_{23}C_6$ carbide films on the grain boundaries, primary MC carbide degeneration and σ-phase formation, all of which have a detrimental effect on creep-resistant properties.[1–8] Most of these changes are reversible, and numerous studies have demonstrated the possibility of the restoration of the blade microstructure and properties after service.[9–16] The implementation of the rejuvenating procedures, such as an appropriate heat treatment and hot isostatic pressing (HIP), has proven to be able to restore even severely overaged microstructure and alloy properties to a practically "as-new" condition, and the procedures are currently employed successfully throughout the industry. However, some service-induced microstructural changes, such as primary MC carbide decomposition, are irreversible, and might affect the aging process after the rejuvenated blades are returned to service. Published data are scarce on the behavior of rejuvenated blades during the next service cycle. The presented study concerns this problem and will discuss the influence of the previous microstructural degradation on the aging kinetics of rejuvenated gas turbine blades made from Ni-based superalloys IN-738 and GTD-111.

E. Lvova and **D. Norsworthy,** Preco and Turbine Compressor Services, Incorporated, Houston, TX 77073. Contact e-mail: glvov@preco-turbine.com.

2. Experimental Procedures

2.1 Materials and Treatments

Four service-exposed blades from four different gas turbines with different service histories were chosen for this study. They will be further referenced as Blade 1, Blade 2, Blade 3, and Blade 4.

Blade 1—first-stage blade from GE MS7001EA turbine, conventionally cast alloy GTD-111.

Blade 2—second-stage blade from GE MS7001B turbine, IN-738 alloy.

Table 1 Chemical compositions of the studied blades

Element	Element content, wt.%			
	Blade 1 (GTD-111)	Blade 2 (IN-738)	Blade 3 (IN-738)	Blade 4 (IN-738)
Carbon	0.095	0.097	0.089	0.110
Chromium	13.78	15.36	16.07	16.39
Cobalt	9.52	8.32	8.52	8.35
Aluminum	2.90	3.48	3.56	3.63
Titanium	4.75	3.31	3.25	3.18
Molybdenum	1.60	1.86	1.84	1.79
Tungsten	3.86	2.65	2.71	2.73
Niobium	…	1.22	1.15	1.07
Tantalum	2.92	1.20	1.42	1.39
Iron	…	0.36	0.29	0.19
Boron	0.014	0.008	0.013	0.014
Silicon	0.019	0.015	0.013	0.009
Nickel	Balance	Balance	Balance	Balance

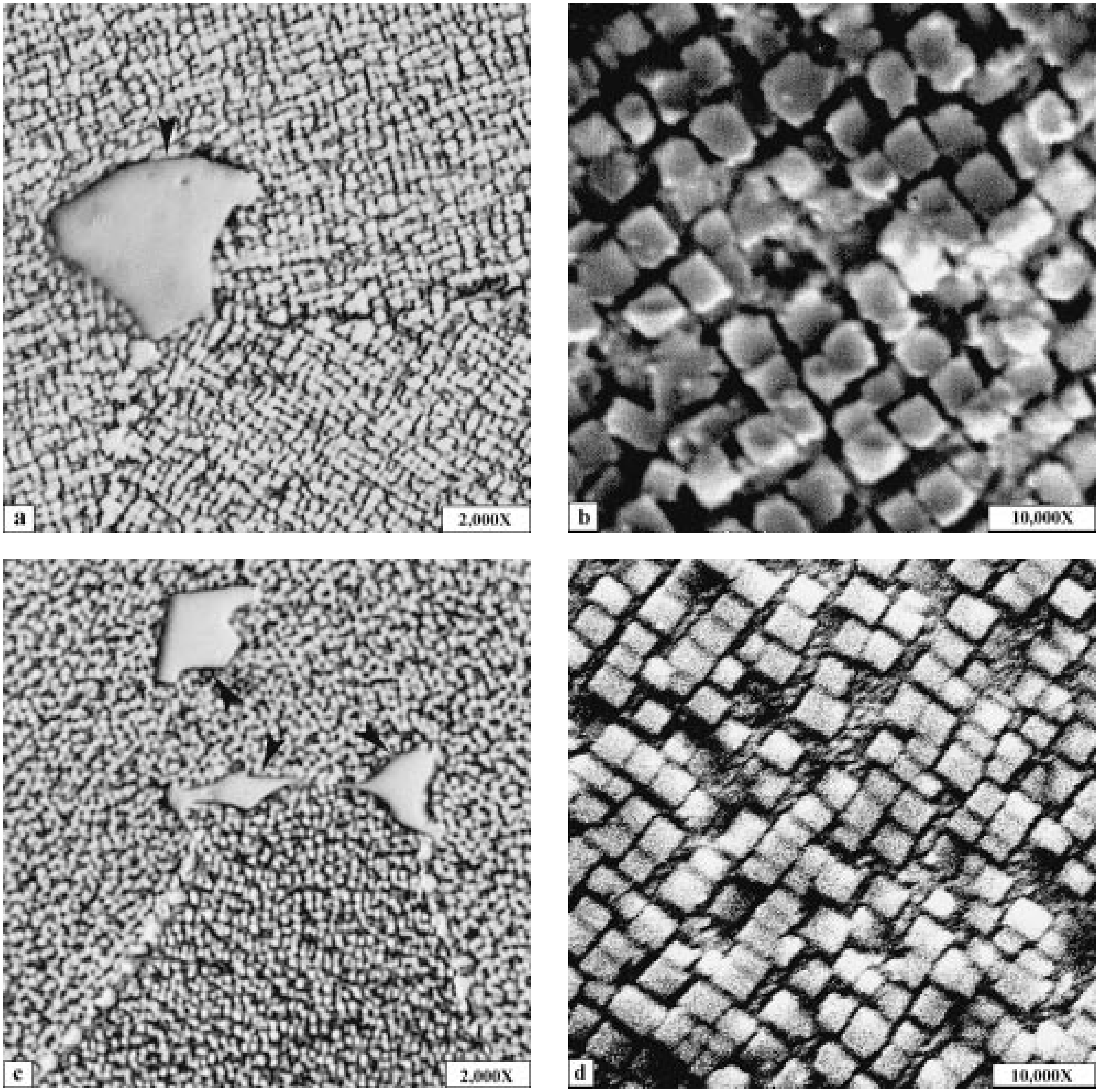

Fig. 1 Microstructure of (**a**) and (**b**) Blade 1 and (**c**) and (**d**) Blade 2 root specimens in the as-received condition. (a) and (c) Optical micrographs and (b) and (d) SEM micrographs. Arrowheads indicate primary MC carbides (etchant—electrolytic chromic acid)

Table 2 Stress-rupture test results of the blades in the as-received condition

	Blade 1		Blade 2		Blade 3		Blade 4	
Specimen location	**Root**	**Airfoil**	**Root**	**Airfoil**	**Root**	**Airfoil**	**Root**	**Airfoil**
Test	815 °C at 480 MPa		815 °C at 450 Mpa		815 °C at 450 MPa		815 °C at 450 MPa	
Time to fracture, h	113.4	15.1	83.8	20.9	74.1	21.3	81.2	31.4
Elongation, %	6.9	4.4	6.5	4.9	7.9	4.3	6.7	4.4
Reduction in area, %	11.6	4.8	9.6	6.7	12.1	6.4	9.9	6.0

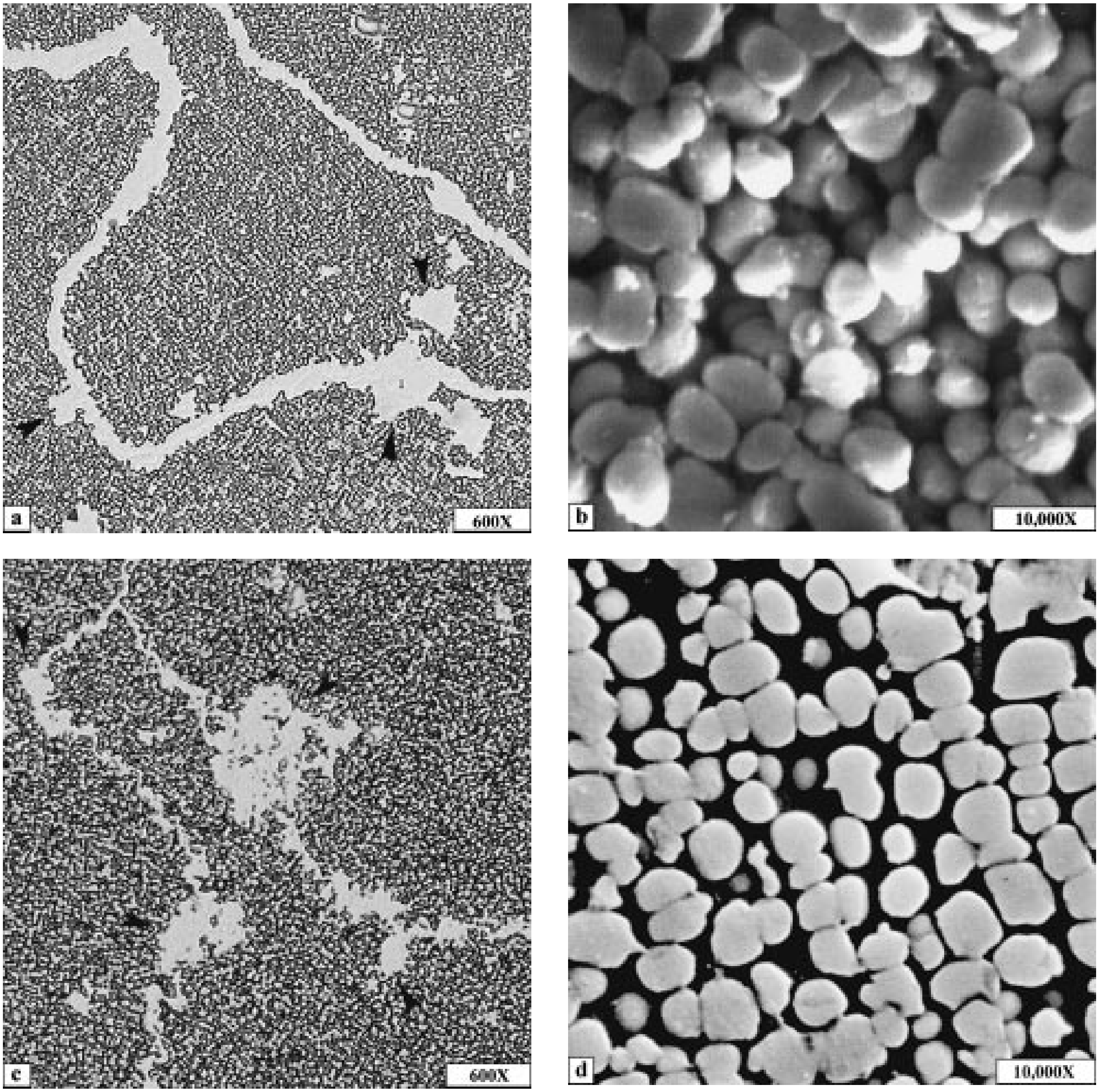

Fig. 2 Microstructure of the (**a**) and (**b**) Blade 1 and (**c**) and (**d**) Blade 2 leading edge specimens in the as-received condition. (a) and (c) Optical micrographs and (b) and (d) SEM micrographs. Arrowheads indicate degenerated primary MC carbides (etchant—electrolytic chromic acid)

Table 3 Microhardness of the blades in the as-received condition

Microhardness H_V							
Blade 1		Blade 2		Blade 3		Blade 4	
Root	Leading edge	Root	Leading edge	Root	Leading edge	Root	Leading edge
429	362	427	354	413	348	392	359

Blade 3—second-stage blade from GE MS7001B turbine, IN-738 alloy.

Blade 4—second-stage blade from GE MS7001E turbine, IN-738 alloy.

The elemental analyses of these blades (except carbon) were performed using an atomic absorption spectrophotometer. Carbon contents were analyzed using a combustion thermal conductivity method. The chemical compositions of the analyzed alloys are given in Table 1.

The blades were sectioned by the wire electric discharge machining (EDM) process at two locations: the root and the

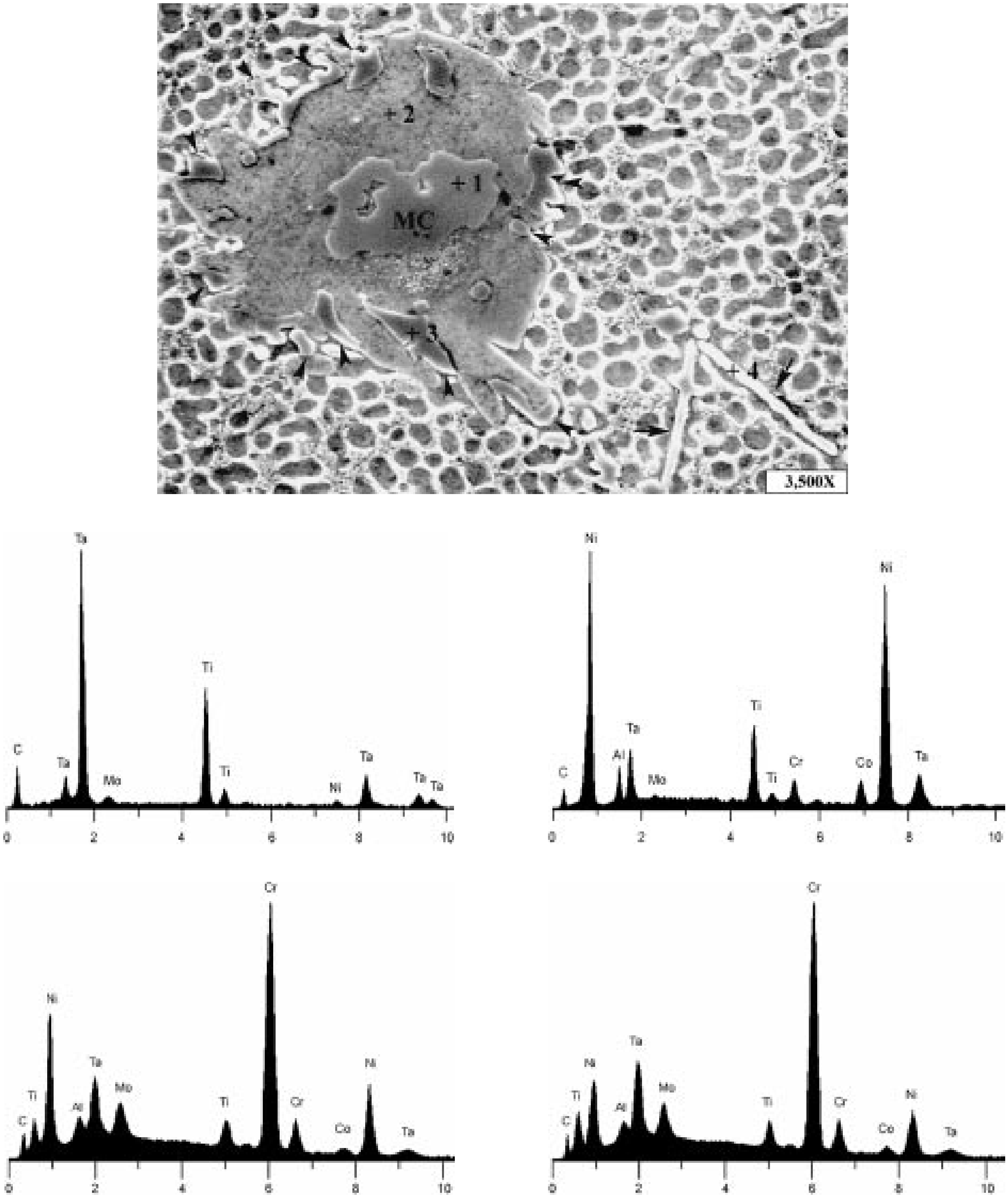

Fig. 3 SEM micrograph and EDX spectra of the degenerated MC carbide in the Blade 1 leading-edge specimen in the as-received condition. $M_{23}C_6$ carbides formed at the edges of the original MC carbide (arrowheads). $M_{23}C_6$ carbides precipitated also in the lathlike morphology (arrows). Energy-dispersive X-ray spectra from marked locations in the micrograph are shown (etchant—Kalling's reagent)

airfoil at approximately one-half airfoil height. The metallographic specimens were cut from the root dovetail and from the leading edge at one-half airfoil height. The specimens for stress-rupture tests were cut from the shank and from the mid-airfoil section. The blade root metal served as an indicator of the initial metal condition, since the service temperature of the

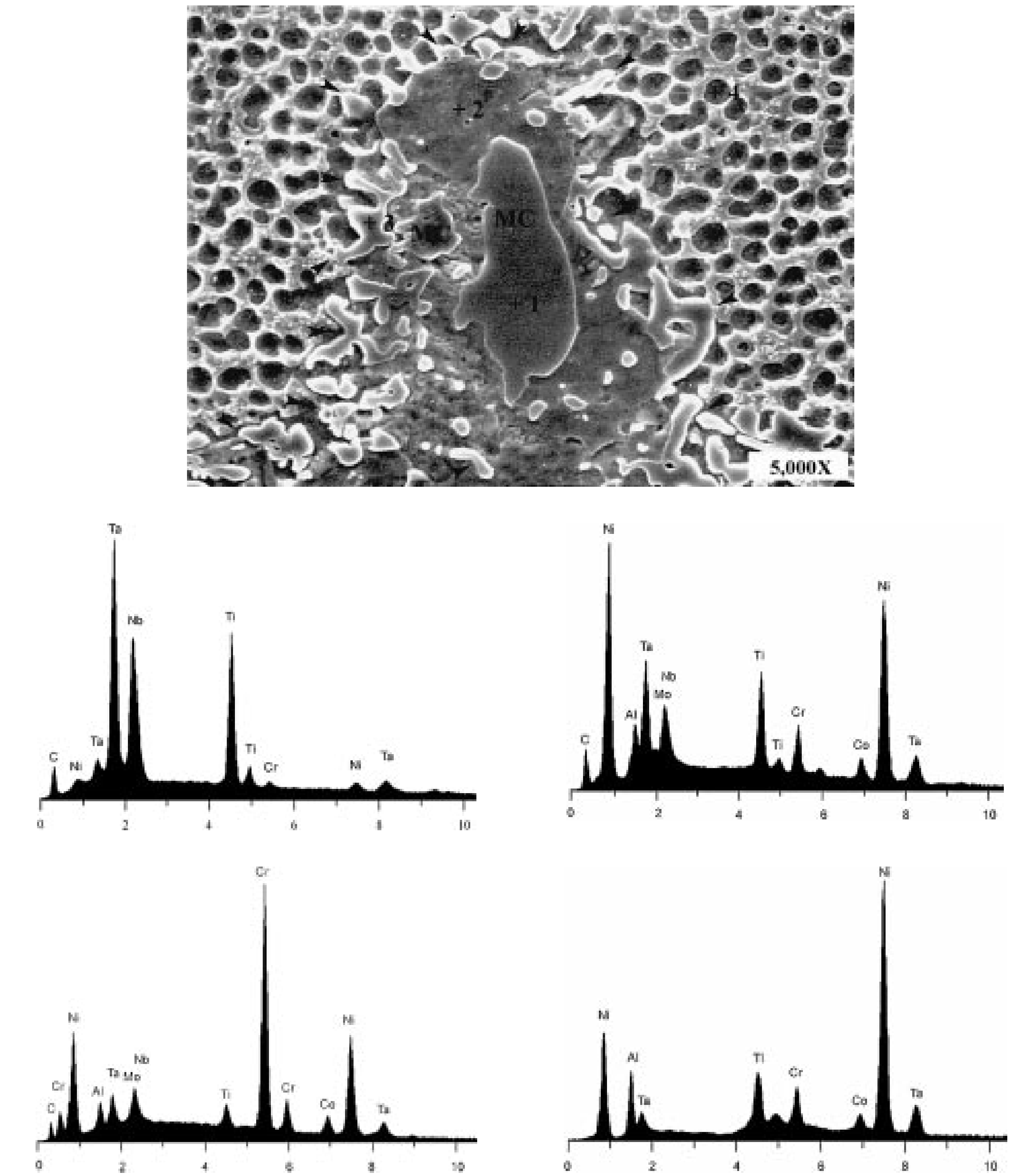

Fig. 4 SEM micrograph and EDX spectra of the degenerated MC carbides in the Blade 2 leading-edge specimen in the as-received condition. Arrowheads indicate $M_{23}C_6$ carbides formed at the edges of the original MC carbides as a result of MC decomposition. Energy-dispersive X-ray spectra from marked locations in the micrograph are shown (etchant—Kalling's reagent)

root is relatively low and does not cause a degradation of the metal microstructure during service. The maximum service-induced damage of the blade material from a combination of high-temperature and operating stresses occurs in the middle of the airfoil (pitch line). The comparison of the microstructure of the blade root and mid-airfoil served to assess service-related

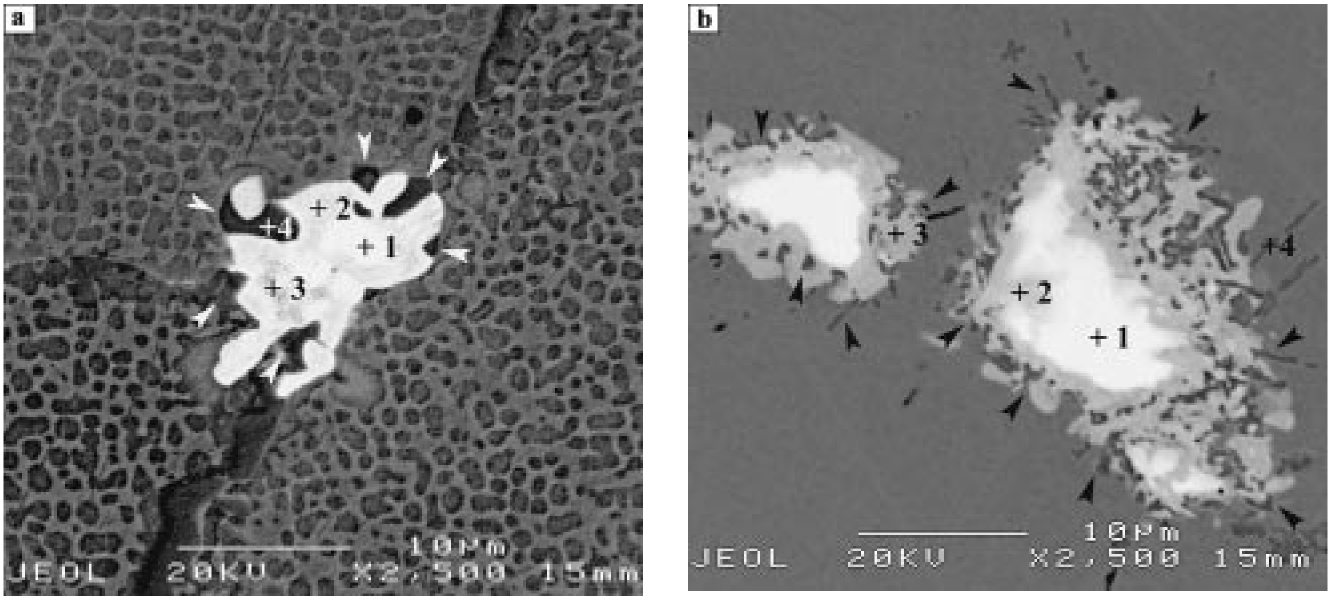

EDS analysis results for Blade 1 leading-edge specimen (BEI micrograph a)								
	Concentration, at.%							
Location	C	Al	Ti	Ta	Mo	Cr	Co	Ni
1	55.7	1.3	17.5	15.6	0.7	0.6	0.8	7.78
2	14.2	7.1	15.5	7.4	0.6	1.7	4.5	49.0
3	13.4	6.9	10.2	8.5	0.5	1.4	5.0	54.1
4	35.2	0.2	1.5	1.8	2.4	47.1	1.8	10.0

EDS analysis results for Blade 2 leading-edge specimen (BEI micrograph b)									
	Concentration, at.%								
Location	C	Al	Ti	Ta	Mo	Nb	Cr	Co	Ni
1	47.4	0.97	18.5	12.3	3.24	8.96	2.48	1.21	4.94
2	26.7	4.31	6.86	9.19	1.36	3.83	6.21	3.14	38.4
3	23.1	2.70	5.91	3.69	0.97	3.61	12.9	5.02	42.1
4	18.9	2.24	2.11	1.24	2.51	0.80	37.4	5.7	29.1

Fig. 5 SEM-BEI micrographs of the degenerated MC carbides in the (**a**) Blade 1 and (**b**) Blade 2 leading-edge specimens in the as-received condition. Dark gray $M_{23}C_6$ carbides (arrowheads) formed on the periphery of MC carbides (light) as a result of the MC decomposition. EDS analysis data from marked locations are shown in the respective tables (as-polished)

changes. One set of specimens was cut from each blade in its as-received condition. The blades then underwent rejuvenation, consisting of HIP and heat treatment specific for the alloy, after which the second set of specimens was cut. The rejuvenating procedures for the studied alloys were.

CC GTD-111: HIP at 1200 °C at 103 MPa of argon, for 4 h, furnace cool
1190 °C for 2 h in vacuum, argon quench
1090 °C for 2 h in vacuum, argon quench
1050 °C for 2 h in vacuum, argon quench
845 °C for 16 h in vacuum, argon quench

IN-738: HIP at 1190 °C at 103 MPa of argon, for 4 h, furnace cool
1180 °C for 2 h in vacuum, argon quench
1120 °C for 4 h in vacuum, argon quench
845 °C for 16 h in vacuum, argon quench

In order to study the aging kinetics after rejuvenation, the blades were aged at 845 °C for 1000 h; interruptions of the aging were made after 200 and 500 h in order to cut the specimens. The temperature of 845 °C was chosen because it falls in the region of the maximum secondary carbide precipitation for the studied alloys.

2.2 Experimental Techniques

The examination of the blade microstructure was performed using optical microscopy and scanning electron microscopy (SEM). Secondary electron imaging (SEI) and backscattered electron imaging (BEI) were used to observe etched and as-polished surfaces. The specimens were etched electrolytically with 10 pct water solution of chromic acid (Cr_2O_3) or chemically with Kalling's reagent (5 g $CuCl_2$ + 3 mL HNO_3 + 50 mL ethanol). An Energy-dispersive spectroscopy (EDS) system

Table 4 Stress-rupture test results after rejuvenation

Specimen location	Blade 1 airfoil	Blade 2 airfoil	Blade 3 airfoil	Blade 4 airfoil
Test	815 °C at 480 MPa	815 °C at 450 MPa	815 °C at 450 MPa	815 °C at 450 MPa
Time to fracture, h	130.9	72.8	69.6	114.9
Elongation, %	7.7	7.3	8.4	7.9
Reduction in area, %	14.6	12.3	12.2	11.9

Table 5 Microhardness of the blades after rejuvenation

Microhardness H_V							
Blade 1		Blade 2		Blade 3		Blade 4	
Root	Leading edge	Root	Leading edge	Root	Leading edge	Root	Leading edge
431	430	429	432	414	416	406	404

with a thin window light element detector was used to determine the elemental distribution of various phases. The microhardness was measured on the metallographic specimens.

Stress-rupture tests were performed according to ASTM E139. The test conditions were chosen based on the creep-rupture curves given in Ref 17 to 19 with the purpose of conducting a test within a reasonable time (approximately 100 h) at a temperature close to the service temperature: 815 °C at 480 MPa—for CC GTD-111 alloy; and 815 °C at 450 MPa—for IN-738 alloy. Short-term 24 h stress-rupture tests at 790 °C at 585 MPa for CC GTD-111 alloy and 760 °C at 585 MPa for IN-738 alloy were also performed. Fracture surfaces of several specimens were examined using SEM.

3. Results and Discussion

3.1 The Blades in the As-Received Condition

The microstructures of the root specimens of Blade 1 and Blade 2 are presented in Fig. 1 (the microstructures of the Blade 3 and Blade 4 root specimens are very similar to that of Blade 2). The root microstructure is typical for a virgin cast superalloy: γ' phase exists in three distinctive morphologies—eutectic lamellar γ' formed between dendrite arms, primary cuboidal γ', and secondary spheroidal γ'; primary MC carbides formed at the grain boundaries and in the interdendritic areas; and fine globular secondary $M_{23}C_6$ carbides decorating the grain boundaries. The micrographs of the Blade 1 and Blade 2 leading edge specimens at one-half airfoil height are presented in Fig. 2 (the microstructures of the Blade 3 and Blade 4 leading edge specimens are very similar to that of Blade 2). Service-induced changes in the leading edge microstructure compared to that of the root are significant and typical for service-exposed gas turbine blades.[1–7,11] The micrographs revealed severe overaging induced by thermal and stress exposure during service. The primary γ' precipitates coarsened considerably at the expense of the secondary γ'; the grain-boundary $M_{23}C_6$ carbide particles coarsened and coalesced, overloading the grain boundaries and forming continuous films at some areas; and primary MC carbides degenerated.

The service-induced deterioration of the airfoil microstructure caused a significant reduction of the stress-rupture life, ductility, and microhardness compared to that of the root. Excessive grain-boundary $M_{23}C_6$ carbide precipitation led to decreasing creep resistance by preventing grain-boundary sliding, initiating void formation, and decreasing overall plasticity. Coarsening and coalescence of γ' precipitates caused a decrease of the tensile strength. The results of the stress-rupture and microhardness tests are presented in Table 2 and 3, respectively.

Special attention was given to a study of the primary MC carbide decomposition, due to the fact that it is an irreversible process and can affect the behavior of a rejuvenated alloy during subsequent service, as well as to the fact that the data on this subject are insufficient. The SEM micrographs of the degenerated MC carbides and energy-dispersive X-ray (EDX) spectra are presented in Fig. 3 and 4. It can be noted that MC decomposition results in a considerable reduction of its size and a formation of numerous $M_{23}C_6$ carbides at the edges of the original MC carbides. $M_{23}C_6$ carbides formed also in the lathlike morphology at the MC periphery as well as in the grain interiors, which was confirmed by EDS analyses. The diminished core of the degenerated MC carbide is surrounded by a smooth-looking substance, which is a product of MC decomposition along with $M_{23}C_6$ carbides (Fig. 3 and 4). The EDS analyses revealed the composition of the primary MC carbides as (Ti, Ta, Mo, Ni, Cr) C in GTD-111 alloy and (Ti, Ta, Nb, Mo, Ni, Cr) C in IN-738 alloy (Fig. 3 to 5). The replacement of the strong carbide forming atoms such as Ti, Ta, and Nb with Mo, Ni, and Cr atoms is known to weaken the interatomic bonds in the MC carbides resulting in a decrease of their stability. This leads to the MC decomposition with a formation of more stable $M_{23}C_6$-type carbides.

The MC carbide decomposition reaction was assumed to be $MC + \gamma \rightarrow M_{23}C_6 + \gamma'$.[3–5,14] $M_{23}C_6$ carbides form at the periphery of the original MC carbides, and the area adjacent to the MC core is supposed to consist of γ' phase. The EDX spectra of the decomposition zone surrounding degenerated MC carbides in the service-exposed Blade 1 and Blade 2 leading edge specimens given in Fig. 3 and 4 did not confirm this assumption. These spectra demonstrate the presence of a substantial amount of carbon, which indicates that the phase from which they were taken cannot be γ'. The comparison of the spectrum from the γ' particle with that from the MC decomposition zone in Fig. 4 illustrates the difference.

The BEI mode of SEM was used to study the microstructure of as-polished specimens, because this method is capable of differentiating microstructural constituents based on their average atomic weight, without the interference of etching. The

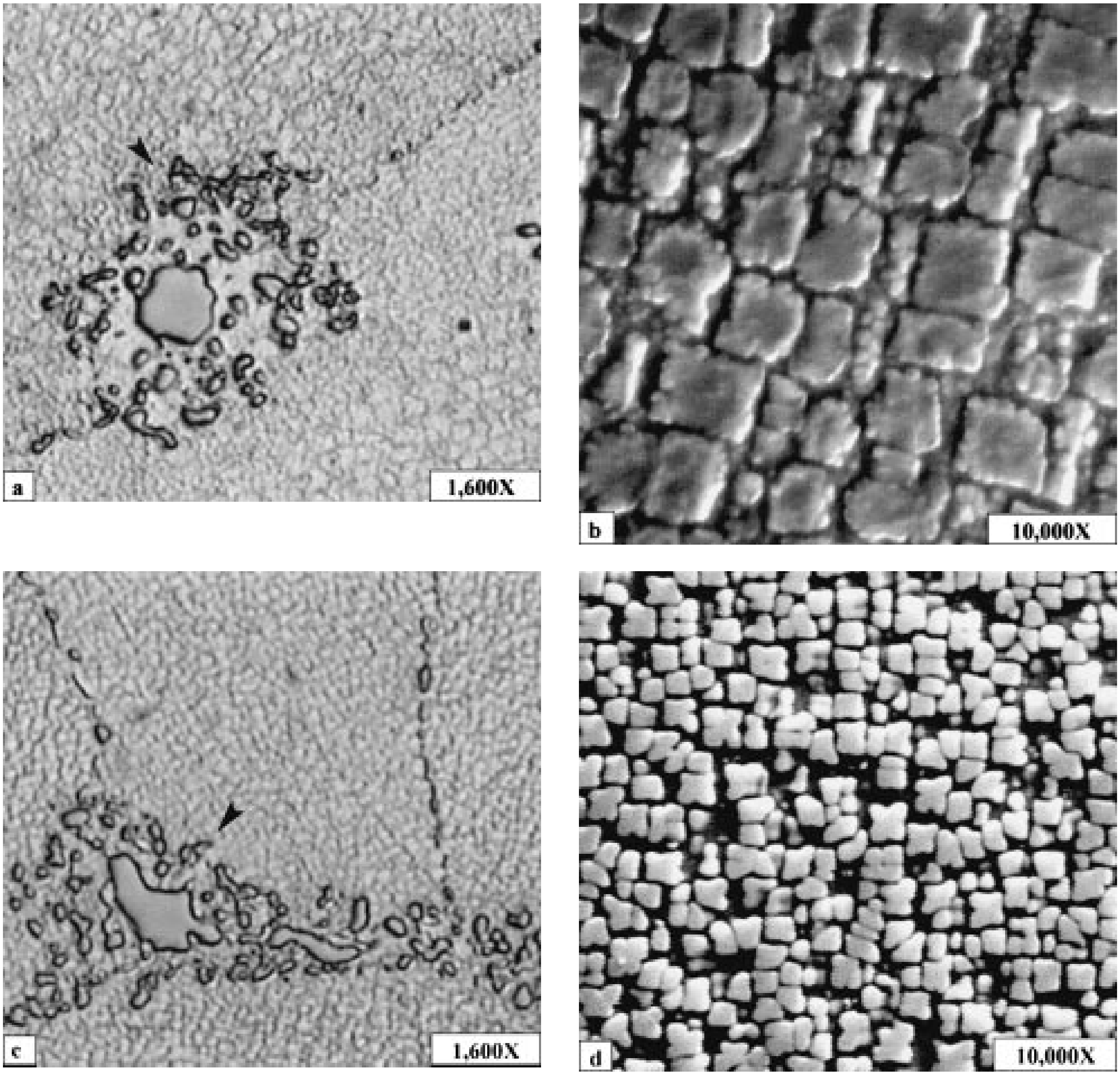

Fig. 6 Micrographs of the (**a**) and (**b**) Blade 1 and (**c**) and (**d**) Blade 2 leading-edge specimens after rejuvenation. (a) and (c) Optical micrographs and (b) and (d) SEM micrographs. Arrowheads indicate disintegrated primary MC carbides (etchants: (a) and (c) Kalling's reagent and (b) and (d) electrolytic chromic acid)

BEI micrographs and the results of EDS analysis of the degenerated MC carbides of GTD-111 and IN-738 alloys are presented in Fig. 5. The BEI micrographs show a presence of dark $M_{23}C_6$ carbides at the MC periphery formed as discrete particles and as laths. A gradual change of the contrast of MC carbide toward its edges can be noted, indicating a change of its chemical composition (it is known that the elemental concentration of MC carbides can vary in a wide range). There is a noticeable difference between γ' contrast and that of the MC decomposition zone. If one of the products of the MC decomposition were γ' phase, it would have had the same contrast as the original γ' phase. This observation allows us to conclude that γ' phase does not form during MC decomposition.

The EDS analysis results show a substantial change of the MC carbide elemental concentration toward its edges; a tendency of carbon content to decrease from the center to the periphery is evident (Fig. 5). Apparently, diffusion of carbon from the metastable MC carbide in to surrounding γ matrix takes place during prolonged thermal exposure, creating a favorable condition for the formation of more stable lower-order $M_{23}C_6$ carbides on the MC/γ interface. The MC carbides serve as a carbon source and γ matrix as a chromium reservoir for the

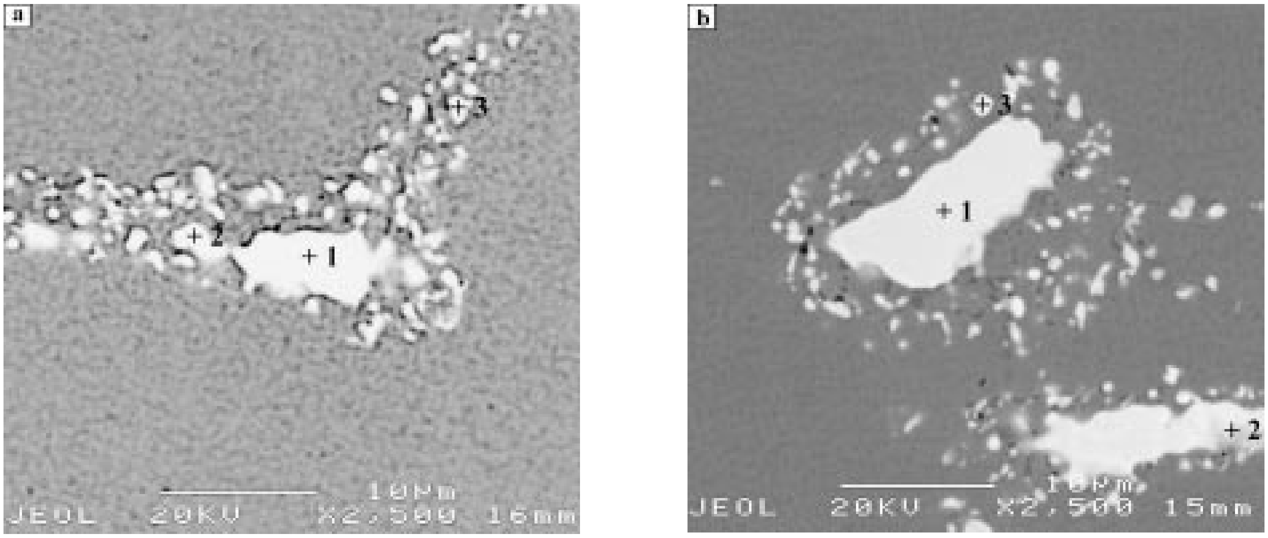

EDS analysis results for Blade 1 leading-edge specimen after rejuvenation (BEI micrograph a)

	Concentration, at.%							
Location	**C**	**Al**	**Ti**	**Ta**	**Mo**	**Cr**	**Co**	**Ni**
1	50.65	2.92	24.05	15.65	0.8	1.1	1.98	2.85
2	27.67	5.95	12.78	9.86	2.45	8.09	2.95	30.25
3	20.94	5.65	3.55	1.92	0.25	13.07	8.25	46.37

EDS analysis results for Blade 2 leading-edge specimen after rejuvenation (BEI micrograph b)

	Concentration, at.%								
Location	**C**	**Al**	**Ti**	**Ta**	**Mo**	**Nb**	**Cr**	**Co**	**Ni**
1	49.16	0.98	18.6	13.9	2.97	9.74	0.93	0.51	3.21
2	38.22	0.71	16.77	11.42	0.36	4.65	2.36	1.83	23.68
3	23.36	4.96	8.13	5.42	0.47	2.88	10.8	6.56	37.42

Fig. 7 SEM-BEI micrographs of the degenerated MC carbides in (**a**) Blade 1 and (**b**) Blade 2 leading after rejuvenation. EDS analysis results from marked locations are shown in the respective tables (as-polished)

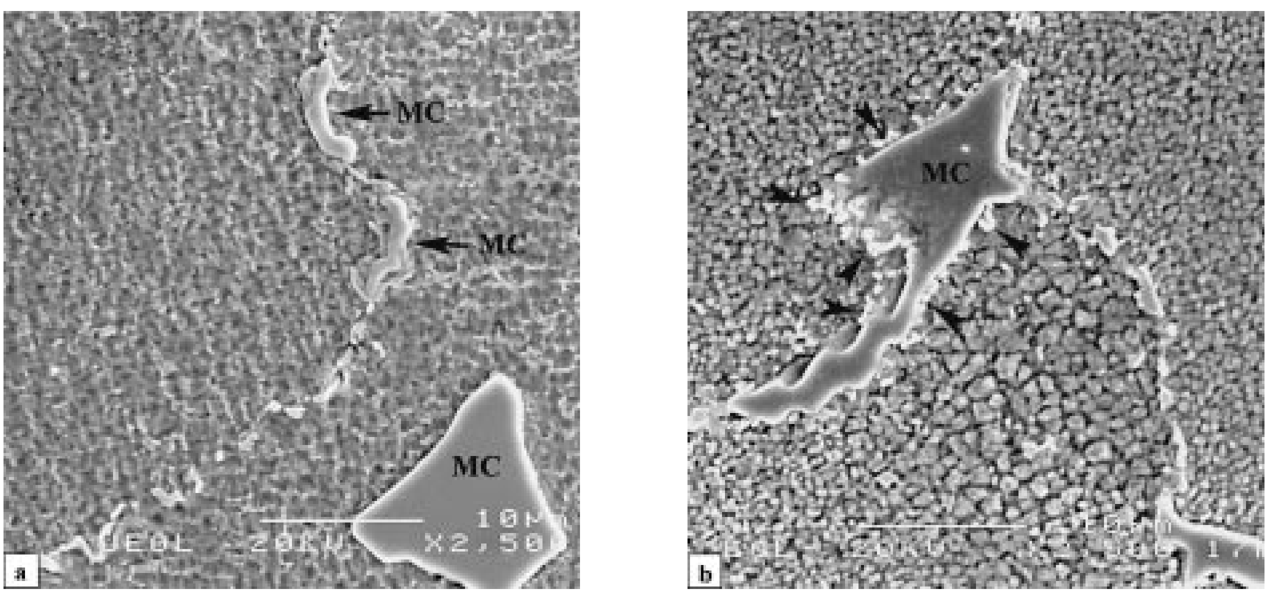

Fig. 8 SEM micrographs of rejuvenated (**a**) Blade 1 and (**b**) Blade 2 root specimens after 1000 h aging at 815 °C. Arrowheads indicated fine $M_{23}C_6$ precipitates at MC carbide edges: (a) BEI (as-polished) and (b) SEI (etchant—Kalling's reagent)

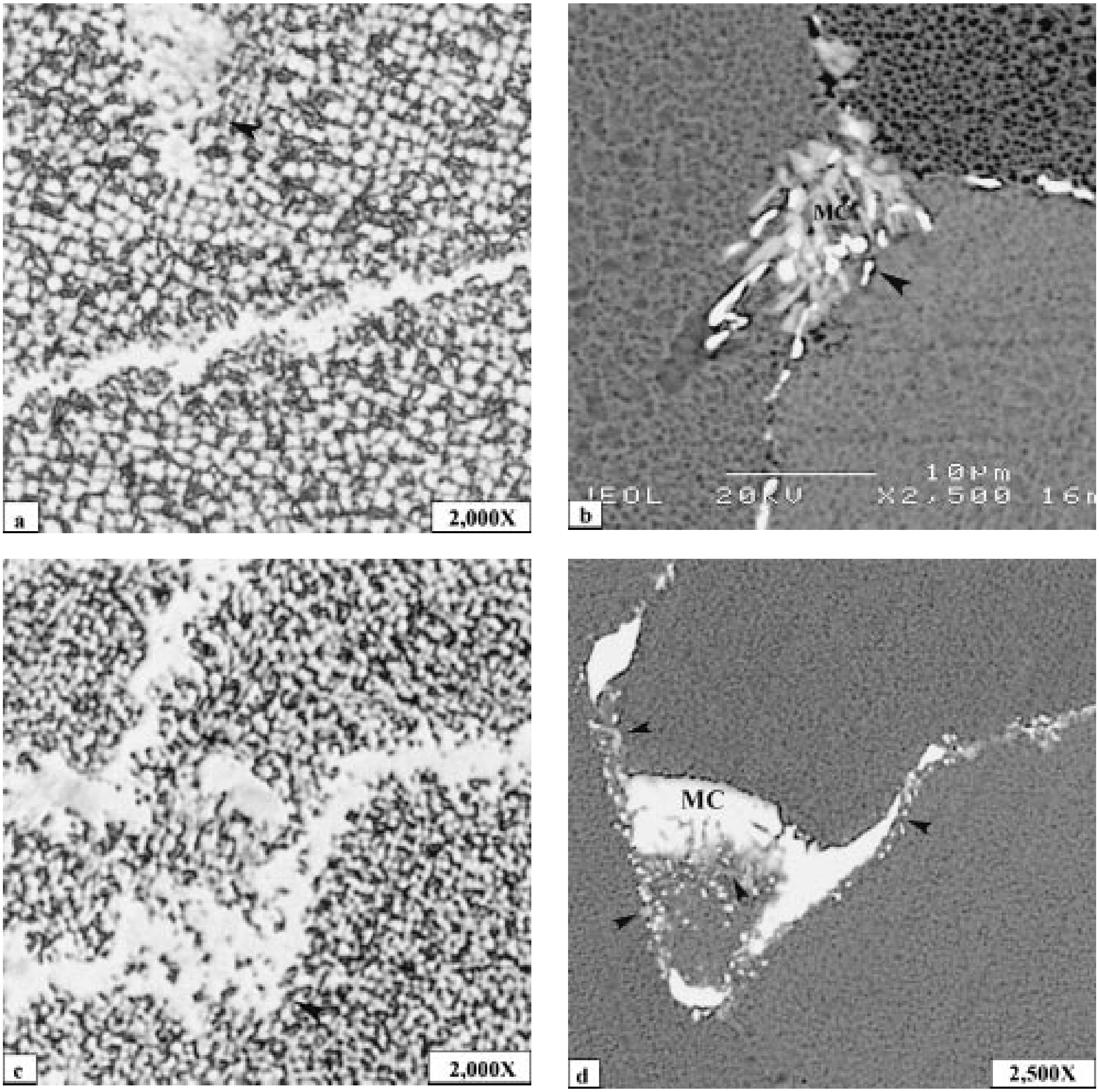

Fig. 9 Micrographs of rejuvenated (**a**) and (**b**) Blade 1 and (**c**) and (**d**) Blade 2 leading-edge specimens after 1000 h aging at 815 °C. Arrowheads indicate previously degenerated MC carbides continuing to deteriorate during aging. (a) and (c) Optical micrographs (etchant—electrolytic chromic acid) and (b) and (d) SEM-BEI micrograph (as-polished)

formation of chromium-rich $M_{23}C_6$ carbides. In light of these findings, the MC decomposition reaction can be informally presented as follows:

$$MC + \gamma \rightarrow M_{23}C_6 + (MC)_{deg}$$

where $(MC)_{deg}$ is a degenerated MC carbide with a reduced carbon content.

It should be noted that primary MC carbides located at or near the grain boundaries demonstrate easier decomposition than do those in the grain interiors. This fact is consistent with the abundance of the grain-boundary $M_{23}C_6$ precipitation. Evidently, the grain-boundary diffusion assists the process of MC decomposition.

3.2 The Blades after Rejuvenation

The rejuvenation of four examined blades was successful in the restoration of the material's properties. Stress-rupture

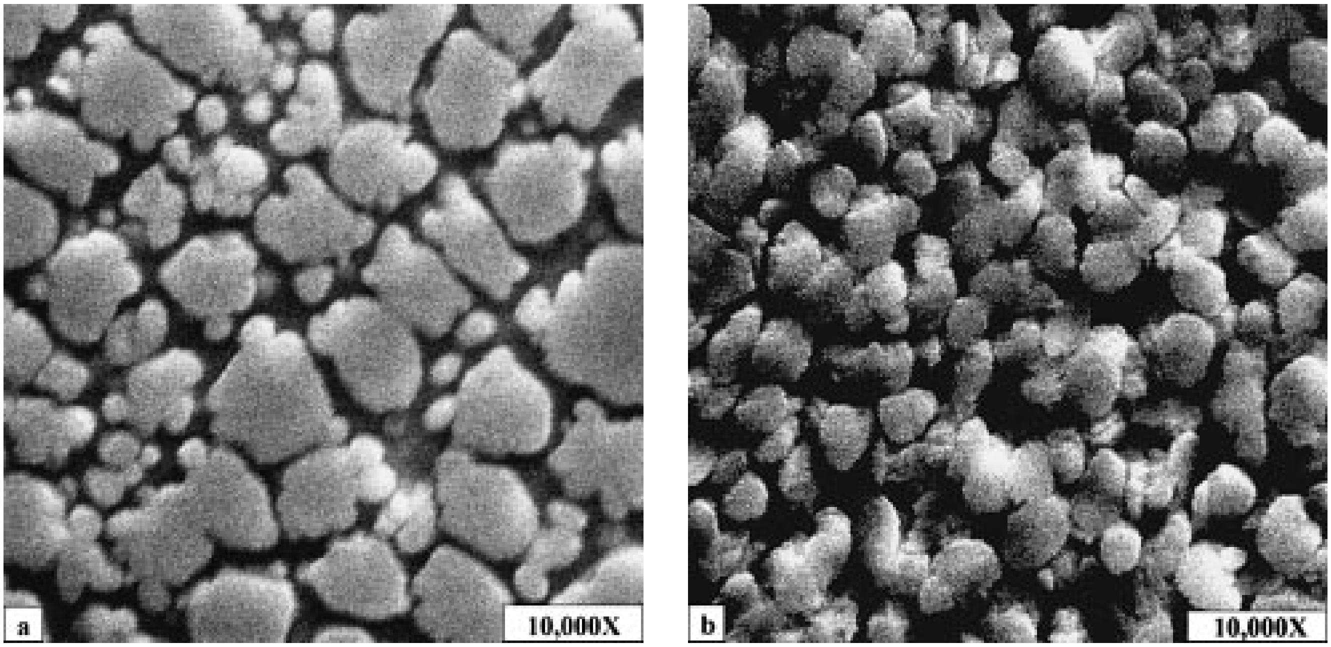

Fig. 10 SEM micrographs of γ' phase in rejuvenated (**a**) Blade 1 and (**b**) Blade 2 leading-edge specimens after 1000 h aging at 815 °C (etchants—electrolytic chromic acid)

life of the mid-airfoil material was dramatically increased, as was the alloy plasticity (Table 4). The microhardness of the leading edge specimens after the rejuvenation also increased significantly, reaching the values of the root (Table 5).

The improvement of the material properties was a result of the restoration of the airfoil microstructure. The micrographs in Fig. 6 reveal the elimination of the excessive grain-boundary carbide precipitation and the refinement of the primary and secondary γ' particles. The morphology of the primary γ' particles is predominantly cuboidal, although not ideally. The microstructure of the rejuvenated leading edge specimens looks similar to that of the root in the as-received condition, except for primary MC carbide morphology: instead of large blocky particles, there are fragments of the original primary carbides present (Fig. 6a and c). The products of the MC carbide decomposition ($M_{23}C_6$ carbides and low-carbon degenerated portions of MC carbides) were dissolved in γ-solid solution during HIP, leaving remnants of original primary MC carbides—unaffected core surrounded with small MC fragments (Fig. 7). The EDS analysis data in Fig. 7 show lower carbon concentrations in the surrounding debris compared to that of the unaffected central part of the original MC carbides. Obviously, dissolved degenerated MC portions had even lower carbon concentration.

Dissolution of the degenerated portions of the primary MC carbides and a profusion of $M_{23}C_6$ carbides formed during the MC decomposition cause a release of additional amounts of carbon into the γ-solid solution. An increased carbon concentration can affect the aging processes occurring in the superalloy and, furthermore, the behavior of the rejuvenated blades in the next service cycle. In order to verify this assumption, we studied the influence of 1000 h aging at 845 °C on the microstructure, microhardness, and stress-rupture life of the rejuvenated blades.

3.3 The Rejuvenated Blades after 1000 h Aging at 845 °C

The effect of aging on the microstructure of the rejuvenated airfoils was compared to that of the root, since the root material showed no primary MC carbide decomposition during service. The micrographs of the rejuvenated root and leading edge specimens after 1000 h aging at 845 °C are presented in Fig. 8 to 10; they reveal a significant acceleration of the aging process in the leading edge compared to the root. While the microstructure of the rejuvenated Blade 1 root is similar to that in the "as-received" condition (practically as new material, Fig. 8a), the Blade 1 leading edge microstructure demonstrates characteristic signs of overaging: excessive secondary carbide precipitation on the grain boundaries and γ' coarsening (Fig. 9a and 10a). The SEM backscattered electron image in Fig. 9(b) shows a change of the contrast of the MC fragments, that is, a previously degenerated MC carbide readily decomposed during aging.

The comparison of the rejuvenated Blade 2 root and the leading edge microstructures after aging shows that they demonstrate a similar tendency, although the aged root specimen reveals a presence of early stages of MC decomposition: the SEM secondary electron image. Figure 8(b) shows a number of very fine globular $M_{23}C_6$ carbides formed around primary MC carbides. The microstructure of the rejuvenated and aged Blade 2 leading edge is typically overaged with the grain boundaries overloaded by $M_{23}C_6$ carbides and coarsened and coalesced γ' (Fig. 9c and d and Fig. 10b). The SEM backscattered electron micrograph in Fig. 9(d) shows gradually changing MC carbide contrast due to additional decomposition of the previously degenerated MC carbides.

The difference in the microstructure of the rejuvenated and aged root and leading edge specimens is reflected in their

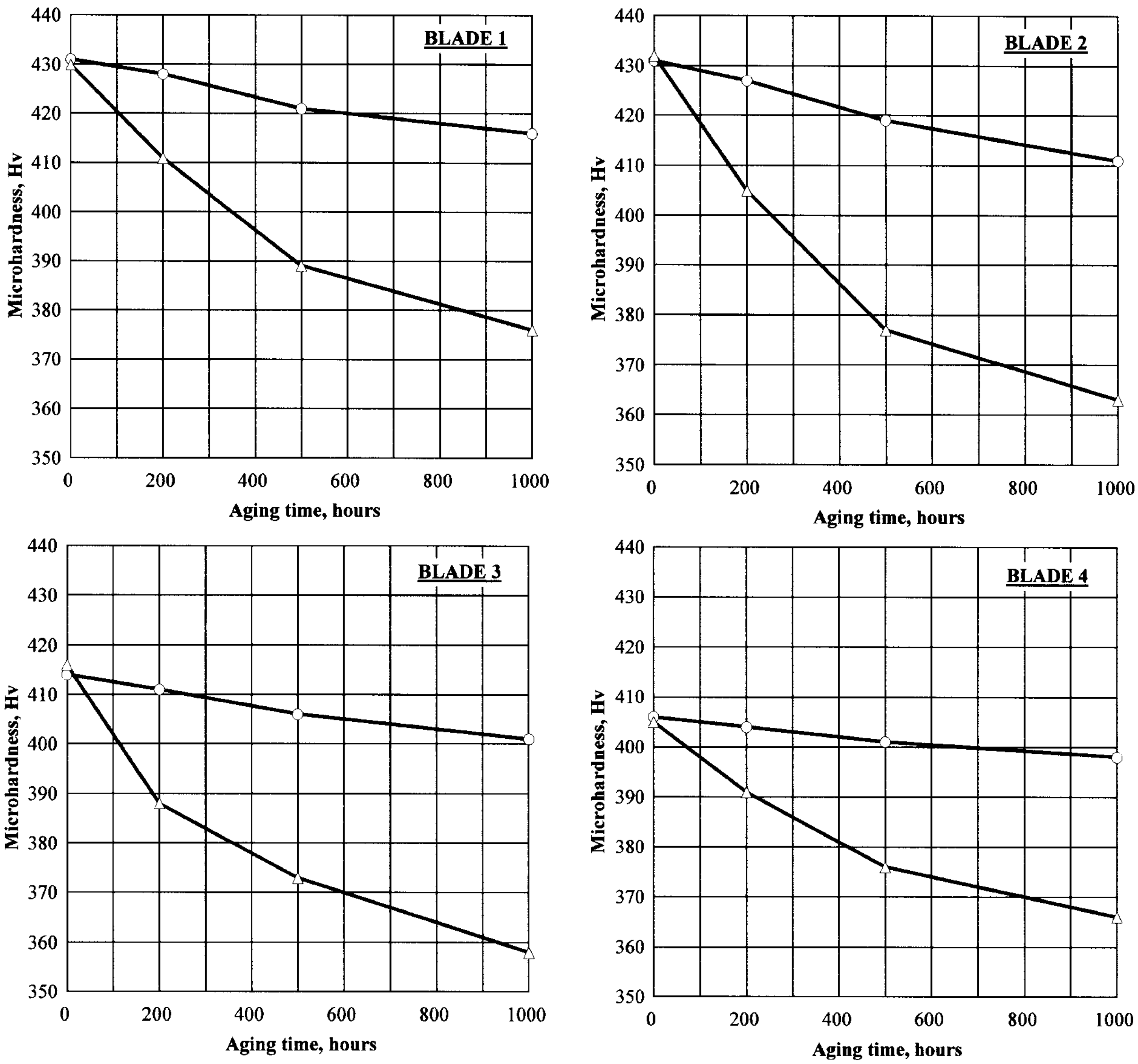

Fig. 11 Influence of aging at 815 °C on the microhardness of rejuvenated blades: ○—root; △—leading edge

microhardness: while the root microhardness decreases slightly, the reduction of the leading edge microhardness is substantial (Fig. 11). The results of the short-term stress-rupture tests also display the difference between rejuvenated and aged root and mid-airfoil behavior. The acceleration of the aging process in the rejuvenated airfoil caused a noticeable reduction of its stress-rupture life and plasticity compared to that of the root (Fig. 12). A comparison of the SEM micrographs of the root and airfoil fracture surfaces illustrates the difference of the fracture mode (Fig. 13). The root specimen from the rejuvenated and aged Blade 4 demonstrates predominantly transgranular ductile fracture, while the fracture surface of the mid-airfoil specimen shows distinct interdendritic-intergranular fracture with a formation of the grain-boundary cavities caused by a heavy secondary carbide precipitation.

The results of the aging experiment demonstrate an obvious effect of the advanced service-induced primary MC carbide decomposition on the aging rate of rejuvenated gas turbine blades. The aging process has evidently accelerated in the mid-airfoil in comparison to the root. The cause of this appears to be the release of additional amounts of carbon into γ-solid solution from dissolution of the MC carbide decomposition products during rejuvenating HIP or solution annealing. The aging acceleration can be expected to be higher when service-induced microstructural deterioration is more advanced, as happens often in modern machines with firing temperatures above 1250 °C, despite the use of protective coatings. In order to extend the blade's life, it seems to be prudent to avoid the extensive primary MC carbide decomposition by reducing the periods between rejuvenations.

4. Conclusions

- Certain service-induced microstructural changes in the Ni-based superalloy, gas turbine blades, such as primary MC

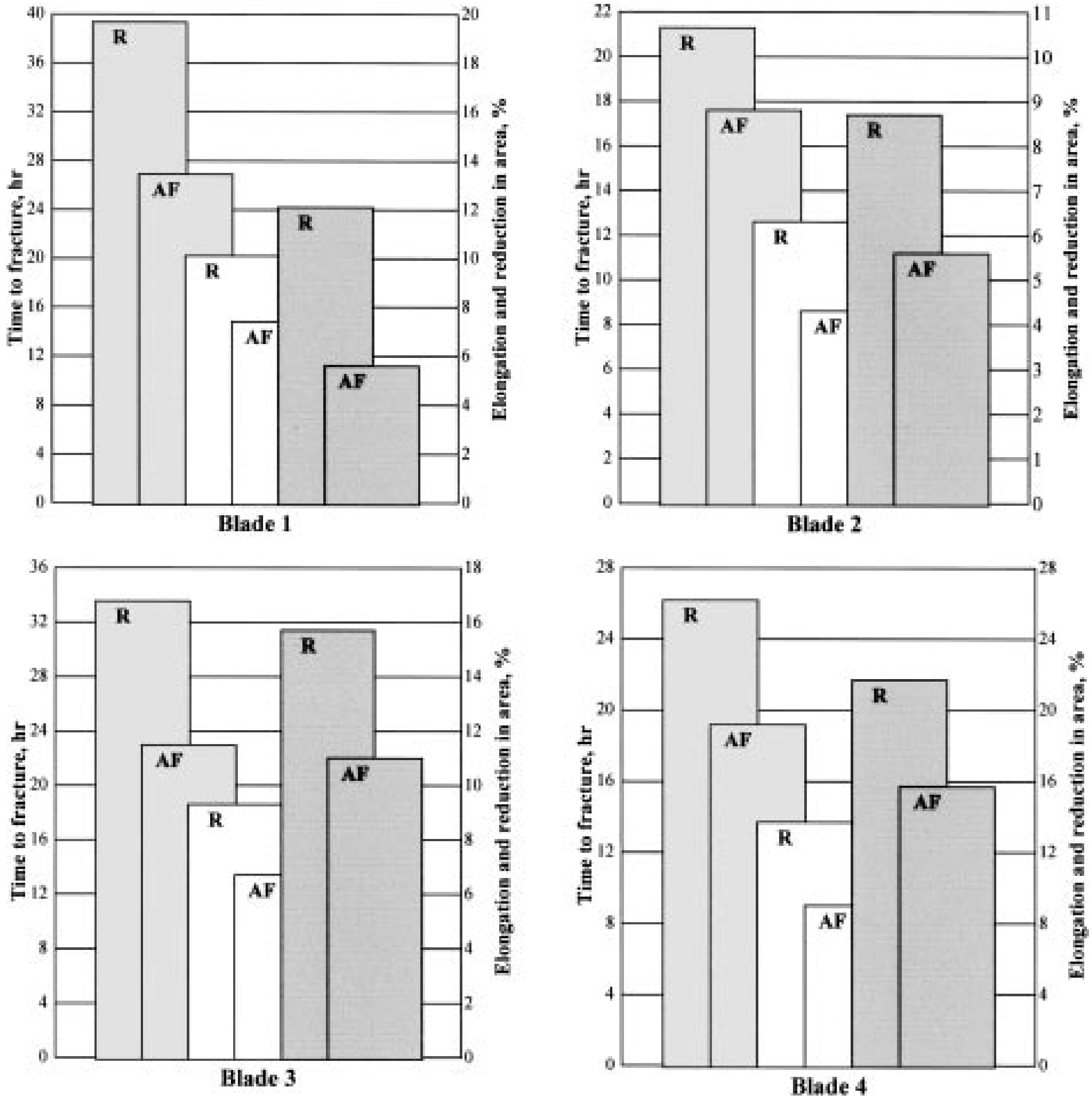

Fig. 12 Results of short-term stress-rupture tests of the rejuvenated blades after 1000 h aging at 815 °C: R—root specimen and AF—airfoil specimen. ▫—time to fracture, h ☐—elongation, % ▪ reduction in area, %

carbide decomposition, are irreversible and were shown in this study to have a significant effect on the aging kinetics of rejuvenated material. An advanced primary MC carbide degeneration leads to the increase of carbon concentration in the γ-solid solution during rejuvenation due to the dissolution of MC carbide decomposition products. This causes the acceleration of the aging of rejuvenated blade airfoils and might affect their performance in the next service cycle.

- The detrimental effect of the MC decomposition can be minimized by reducing the periods between rejuvenations.
- The detailed study of the primary MC carbide decomposition processes has been conducted. It was found that MC decomposition during thermal exposure follows the reaction

$$MC + \gamma \rightarrow M_{23}C_6 + (MC)_{deg}$$

where $(MC)_{deg}$ is a degenerated MC carbide with a reduced carbon content.

- The subject of this study is very complex and requires further investigation, in order to better understand the processes occurring in the rejuvenated gas turbine blades.

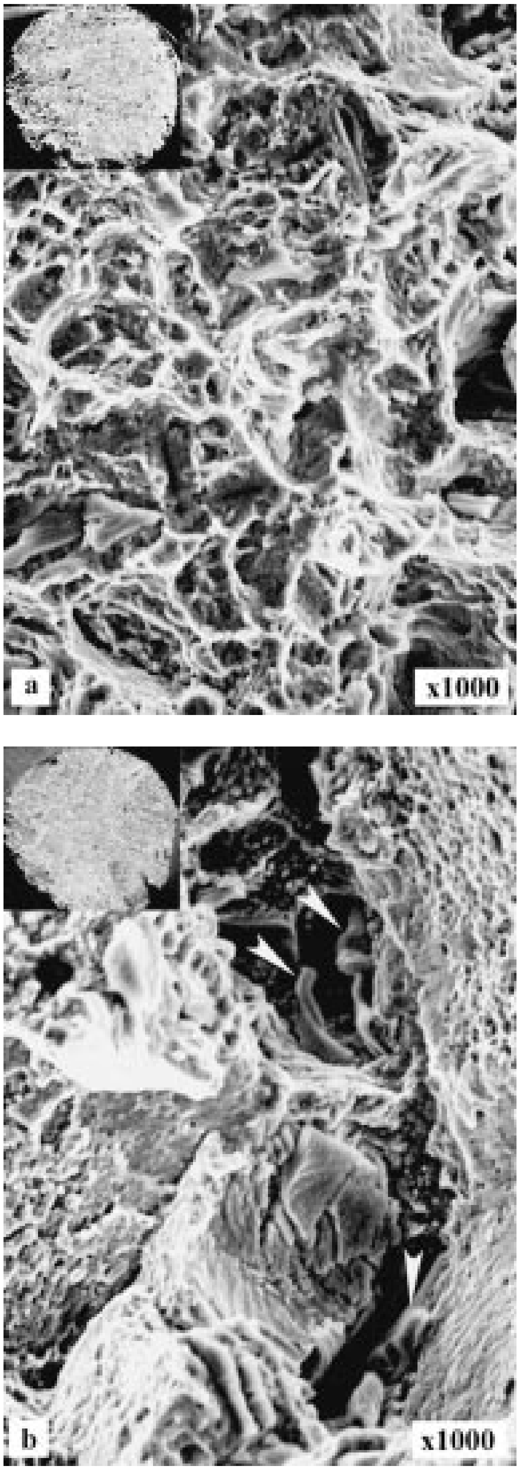

Fig. 13 SEM-micrographs of the fracture surfaces of rejuvenated and aged Blade 4 (**a**) and (**b**) root and (**c**) and (**d**) airfoil specimens. Arrowheads indicate grain-boundary cavities formed due to heavy $M_{23}C_6$ carbide precipitation

Acknowledgments

The authors thank Drs. V. Levit and R. Crooks, Black Laboratories, L.L.C., for valuable discussions during the course of this work.

References

1. R.A. Stevens and P.E.J. Flewitt: *J. Mater. Sci.,* 1978, vol. 13, pp. 367-76.
2. R.A. Stevens and P.E.J. Flewitt: *Mater. Sci. Eng.,* 1979, vol. 37, pp. 237-47.
3. R. Castillo and A.K. Koul: *Proc. Conf. "High Temperature Alloys for Gas Turbines and Other Applications,"* Liege, Belgium, Oct. 6–9, 1986, pp. 1395-1410.
4. E.W. Ross and C.T. Sims: in *Superalloys II,* C.T. Sims, N.S. Stoloff, and W.C. Hagel, eds., John Wiley & Sons, New York, NY, 1984, pp. 112-16.
5. A.K. Koul and R. Castillo: *Proc. ASM 1993 Materials Congr.,* Materials Week '93, Pittsburgh, PA, Oct. 17–21, 1993, ASM International, Materials Park, OH, 1994, pp. 75-88.
6. H.M. Tawancy, N.M. Abbas, A.I. Al-Mana, and T.N. Rhys-Jones: *J. Mater. Sci.,* 1994, vol. 29, pp. 2445-58.
7. Huang Xuebing, Kang Yan, Zhou Huihua, Zhang Yun, and Hu Zhuangqi: *Mater. Lett.,* 1998, vol. 36, pp. 210-13.
8. J.A. Daleo and J.R. Wilson: *J. Eng. Gas Turbines and Power,* 1998, vol. 120, ASME paper no. 96-GT-520.
9. R.A. Stevens and P.E.J. Flewitt: *Strength of the Metals and Alloys,* 5th Int. Conf., Aachen, Germany, Aug. 27–31, 1979, Pergamon Press, Elmsford, NY, 1979, vol. 1, pp. 439-44.
10. J.C. Beddoes and W. Walace: *Metallography,* 1980, vol. 13, pp. 185-94.
11. P.H. Floyd, W. Wallace, and J.-P.A. Immarigeon: *Proc. Conf. "Heat Treatment '81,"* Birmingham, England, Sept. 15–16, 1981, The Metals Society, London, 1983, pp. 97-102.
12. A.K. Koul and R. Castillo: *Metall. Trans. A,* 1988, vol. 19A, pp. 2049-66.
13. W.B. Busch and J. Wortmann: *Proc. Conf. "Material Development in Turbo-Machinery Design,"* Cambridge, United Kingdom, Sept. 12–14, 1988, The Institute of Metals, London, 1989, pp. 151-57.
14. T.M. Maccagno, A.K. Koul, J.-P. Immarigeon, L. Cutler, R. Allem, and G. L'Esperance: "Rejuvenation of Service Exposed Alloy 713C Turbine Blades," Report of National Aeronautical Establishment, National Research Council, Ottawa, Ontario, Canada, July 26, 1989.
15. A. Baldan: *Proc. Conf. "Materials Aging and Component Life Extension,"* Milan, Italy, Oct. 10–13, 1995, Engineering Materials Advisory Services Ltd., United Kingdom, 1995, vol. II, pp. 943-50.
16. J. Hakl, V. Bina, J. Kudrman, and R. Pech: *Proc. Conf. "Materials Aging and Component Life Extension,"* Milan, Italy, Oct. 10–13, 1995, Engineering Materials Advisory Services Ltd., United Kingdom, 1995, vol. II, pp. 991-1000.
17. *Aerospace Structural Metals Handbook,* CINDAS/USAF CRDA Handbooks Operation, Purdue University, West Lafayette, IN, 1998, vol. 5.
18. *Atlas of Creep and Stress-Rupture Curves,* ASM International, Materials Park, OH, 1998.
19. *Heat-Resistant Materials,* ASM International, Materials Park, OH, 1997.